FLEXIBLE DEVICES

Liquid metal-based soft, hermetic, and wireless-communicable seals for stretchable systems

Qingchen Shen^{1,2}†, Modi Jiang^{1†}, Ruitong Wang^{1†}, Kexian Song^{1†}, Man Hou Vong^{2†}, Woojin Jung², Febby Krisnadi², Ruyu Kan¹, Feiyu Zheng¹, Benwei Fu¹, Peng Tao¹, Chengyi Song¹, Guoming Weng³, Bo Peng⁴, Jun Wang^{5*}, Wen Shang^{1*}, Michael D. Dickey^{2*}, Tao Deng^{1,3*}

Soft materials tend to be highly permeable to gases, making it difficult to create stretchable hermetic seals. With the integration of spacers, we demonstrate the use of liquid metals, which show both metallic and fluidic properties, as stretchable hermetic seals. Such soft seals are used in both a stretchable battery and a stretchable heat transfer system that involve volatile fluids, including water and organic fluids. The capacity retention of the battery was ~72.5% after 500 cycles, and the sealed heat transfer system showed an increased thermal conductivity of approximately 309 watts per meter-kelvin while strained and heated. Furthermore, with the incorporation of a signal transmission window, we demonstrated wireless communication through such seals. This work provides a route to create stretchable yet hermetic packaging design solutions for soft devices.

he rapid advancement of stretchable canned goods and liners in packaging (such electronics reactive species, such as recently (8–11). Their metallic electric con-

oxygen and water, away from sensitive materials and thereby ensure the long-term stability of the devices. There is, however, no equivalent stretchable packaging that provides a hermetic seal for stretchable devices and systems (4-7). Stretchable materials, such as elastomers, have large free volume and high chain mobility and therefore readily permeate gases. Consequently, materials with a low Young's modulus generally have high gas permeability (6, 7). The current approaches to addressing such challenges involve combining materials that have low Young's modulus, such as elastomers, with materials that have low gas permeability, such as inorganic or metallic materials, but these approaches show either limited stretchability or limited hermetic performance.

Liquid metals (LMs) have both metallic and fluidic properties and thus provide an opportunity to achieve stretchable and hermetic sealing. Metals, such as aluminum and steel, are known as excellent permeation barriers and therefore find use in the food industry in

promises to enable new types as potato chip bags). Yet, metals are generally of humanmachine interfaces and soft inextensible. LMs, especially gallium and its devices (1-3). Conventional rigid elec- alloys, are an exception that have attracted intronic devices are encased in packaging creased attention from the research community materials to keep

> ductivity and fluidic deformability make them suitable for applications in stretchable and soft electronics (8, 12, 13). Their metallic thermal conductivity and fluidic deformability also offer the potential of using them as thermal interface materials (14, 15) for dissipating heat from electronic devices. LMs should also have similar hermetic sealing performance as that of metals, while at the same time show Young's modulus much lower than that of the common elastomers that have limited hermetic performances (Fig. 1A). Such a combination of low Young's modulus and low gas permeability makes LMs ideal candidates for the generation of stretchable and hermetic seals.

> We studied the hermetic performance of LMs and demonstrated a stretchable and hermetic seal enabled by LMs with the integration of spacers. A common LM, eutectic gallium indium (EGaIn), was used in this study.

Gas permeability of LMs

To measure the gas permeability of EGaIn, we

State Key Laboratory of Metal Matrix Composites, School of Materials Science and Engineering, Shanghai Jiao Tong University, Shanghai 200240, P. R. China, ²Department of Chemical and Biomolecular Engineering, North Carolina State University, Raleigh, NC 27695, USA. 3Shanghai Key Laboratory of Hydrogen Science, School of Materials Science and

fabricated a barrier film (fig. S1A) by filling a

P. R. China. ⁴Wanxiang A123-Global Headquarters, A123 Systems, Hangzhou 311215, P. R. China. 5Research and Development Center A123 Systems, Waltham, MA 02451, USA *Corresponding author. Email: dengtao@situ.edu.cn (T.D.); mddickey@ncsu.edu (M.D.D.); shangwen@situ.edu.cn (W.S.); jwang.a123systems@gmail.com (J.W.)

Engineering, Shanghai Jiao Tong University; Shanghai 200240,

†These authors contributed equally to this work. chamber with EGaIn by the method of vacuum (OTR) permeation analyzer (OX-TRAN 2/22H, AMETEK MOCON) to measure the oxygen permeability.

The permeability, P, is defined by the following equation (7)

> J h ðÞ P 1/4 1 s Dp

where J is the gas flux through the sample per unit time, h is the thickness of the sample, s is the surface area of the sample, and Dp is the difference of gas pressure between two sides of the sample.

Because of the low gas permeability of glass (7), the water and oxygen flux in the area with glass can be neglected. The part with EGaIn is a three-layer laminate structure that includes two layers of polydimethylsiloxane (PDMS) and one layer of EGaIn. When the gas flux reaches the steady state, the gas flux through each layer is the same, and Eq. 1 can be converted to Eq. 2

Dptot ¼ DpPDMS 1 bDpEGaIn bDpPDMS 2

Lhpdms , hegain hpdms 2 1/4 s Ppdms

þPEGaIn þ PPDMS ðÞ

2

where hpdms_1, hpdms_2, and hegain are the thickness of the corresponding layers, and

P_{PDMS} and P_{EGaIn} are the permeability of PDMS and EGaIn, respectively.

As shown in fig. S2A, the water flux through the sample with EGaIn reached a stable value, 4.0×10^{-7} cc/day, after about 94-hour measurement. This value is at the lower measurement limit of the WVTR permeation analyzer

perme vapor transm (AQU. measu placed partial flux th an oxy

filling

Shen et al., Science 379, 488-493 (2023) 3 February 2023 1 of 6 $[(2.5 \pm 2.5) \times 10^{-7} \text{ cc/day}]$. P_{EGaln} of water was calculated to be $9.6 \times 10^{-21} \text{ m}^2/\text{(s Pa)}$, which is more than four orders of magnitude smaller than that of PDMS (6). The actual permeability of EGaIn may be smaller than the measured value if an instrument with better sensitivity can be used. As shown in fig. S2B, the oxygen flux through the sample with EGaIn reached 2.5×10^{-6} cc/day, which also reaches the measurement limit of the OTR permeation analyzer

 $[(2.5 \pm 2.5) \times 10^{-6} \text{ cc/day}]$. P_{EGaIn} of oxygen was calculated to be $5.0 \times 10^{-23} \text{ m}^2/(\text{s Pa})$, which is more than eight orders of magnitude smaller than that of PDMS (17).

Gas permeability versus Young's modulus for various stretchable materials are plotted in Fig. 1, B and C (7). In Fig. 1, B and C, the solid red dots indicate the measured values for EGaIn. The permeability of oxygen is measured to be close to that of metal [aluminum (Al)]. The permeability of water is relatively high compared with that of metal (Al), which is primarily due to the current limitation of the instrument we used for the water permeability measurement.

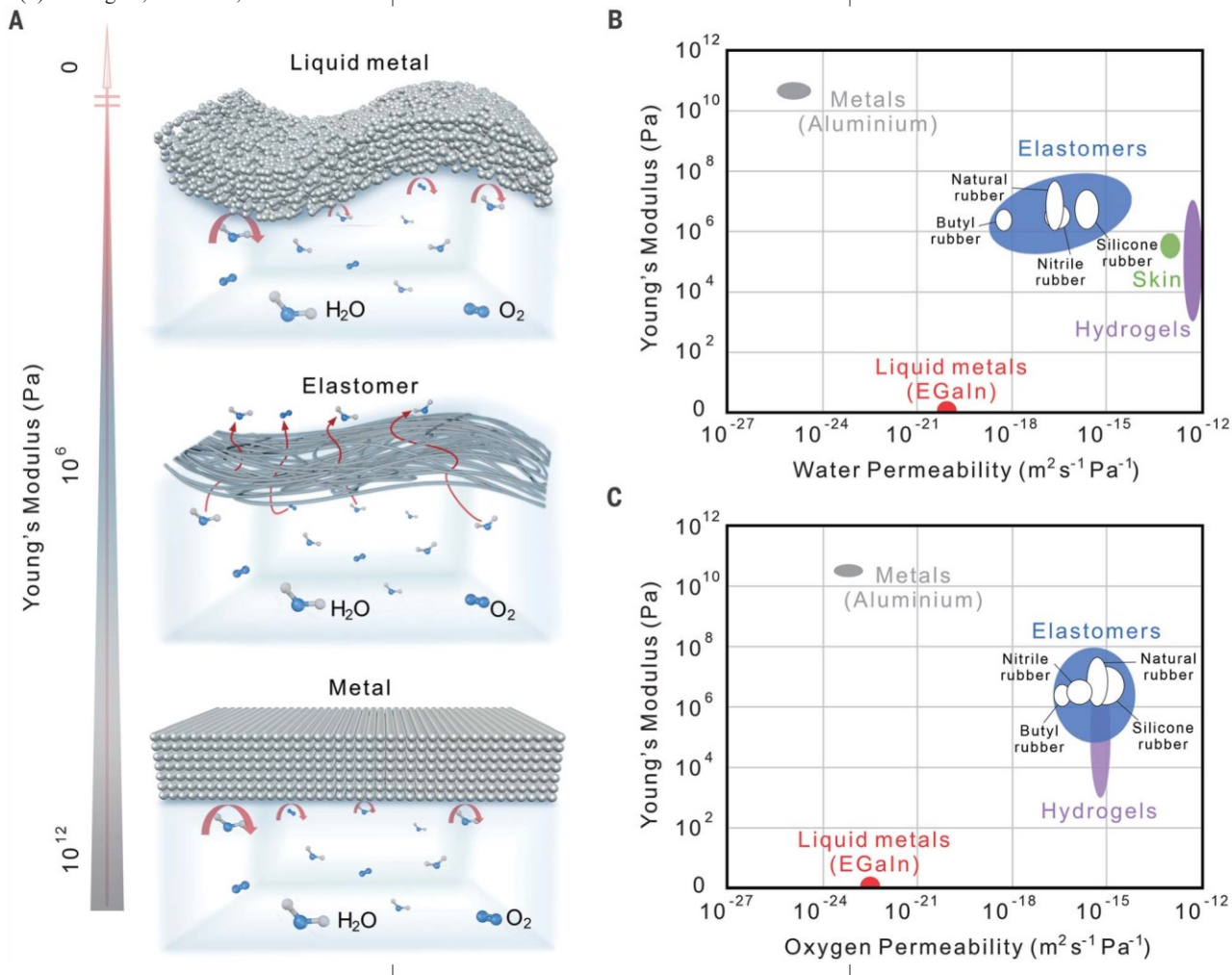


Fig. 1. Gas permeability of LMs. (A) Schematic of methanical and hermetic properties of metals, elastomers, and LMs. Metals generally have rigidity Young's modulus) and low gas permeability. Elastomers have elasticity Young's modulus) and high gas permeability. LMs show both fluidity (effectively zero Young's modulus) and gas permeability that is as low as that (AI) is included as a reference in (B) and (C).

 $\mbox{LM-based}$ soft and hermetic seals $\mbox{With the low gas}$ permeability and soft mechanical properties, EGaIn opens possible design space to achieve stretchable and hermetic seals, which will help enable the practical long-term applications of stretchable and soft systems that are sensitive to the permeation of various gases, including flexible electronics systems, wearable systems, energy generation and storage systems, heat

transfer systems, sensing systems, and biomedical systems (18-25). In this work, we demonstrated the design and fabrication of LMbased seals with the integration of spacers for stretchable batteries-specifically, lithium-ion batteries (LIBs) with a water-based electrolyte. Most research in stretchable batteries focuses on the stretchable current collector (26), electrode (27), and electrolyte (28). The stretchable

of other metals. (B) Young's modulus versus water permeability for various stretchable materials. (C) Young's modulus versus oxygen permeability for (high various stretchable materials. Except the data of EGaIn, the data points (low for all materials in (B) and (C) are from (7). A common metal barrier material

> packaging, which plays a critical role in the longterm stability and safe operation of the stretchable batteries, is usually overlooked, with limited performance reported (4, 5).

Shen et al., Science 379, 488-493 (2023) 2 of 6 3 February 2023

RESEARCH | RESEARCH ARTICLE

The exploded schematic in Fig. 2A shows the key components integrated into the stretchable LIB with the LM-based seal. The inner cell in Fig. 2B is a stretchable LIB without a LM-based seal. There are three steps in the fabrication of the LM-sealed LIB: fabrication of the electrodes (fig. S3A), fabrication of the inner cell (fig. S3B), and fabrication of the outer seal (fig. S3C). In the fabrication of the electrodes (fig. S3A), the premixed slurries of cathode materials, which are based on commercial lithium manganese oxide, were coated onto the current collector of stainless steel meshes through the blade coating process. The premixed slurries of anode materials, which are based on carboncoated lithium titanate phosphate (cc-LTP) (fig. S4) (29), were coated onto stainless steel meshes by using a similar process. The fabricated electrodes were then cut into strips with a size of 45 by 3 mm, which were wrapped by a hydrophilic porous polytetrafluoroethylene (PTFE) separator to avoid internal shortcircuiting. The obtained electrodes were further connected with stainless steel tabs for the performance characterization. For the integration of the LM-based seal, parts of the stainless steel tabs that were in contact with LM were precoated with a thin layer of parylene (~10 mm in thickness) to prevent the LMinduced short-circuiting between the tabs. The assembled electrodes were attached onto a PDMS substrate

Fig. 2. Stretchable and hermetic seals for LIBs. (A) Exploded schematic showing the key components of the LM-based seal that is integrated into the stretchable LIB. (B) Schematic configuration of the inner cell of the stretchable LIB. (C) Photograph of the stretchable LIB with the LM-based seal. (D and E) Optical microscopy images of patterned glass beads on a PDMS sheet from (D) the top view and (E) the cross-sectional view. (F) Photograph of the LIB with the LM-based seal under no stretching. (G) Photograph of the LIB with the LM-based seal under stretching. (H) Mass change of LIBs with and without the LM-based seal. The inner cells for both LIBs were filled with a waterbased electrolyte.

Shen et al., Science 379, 488-493 (2023

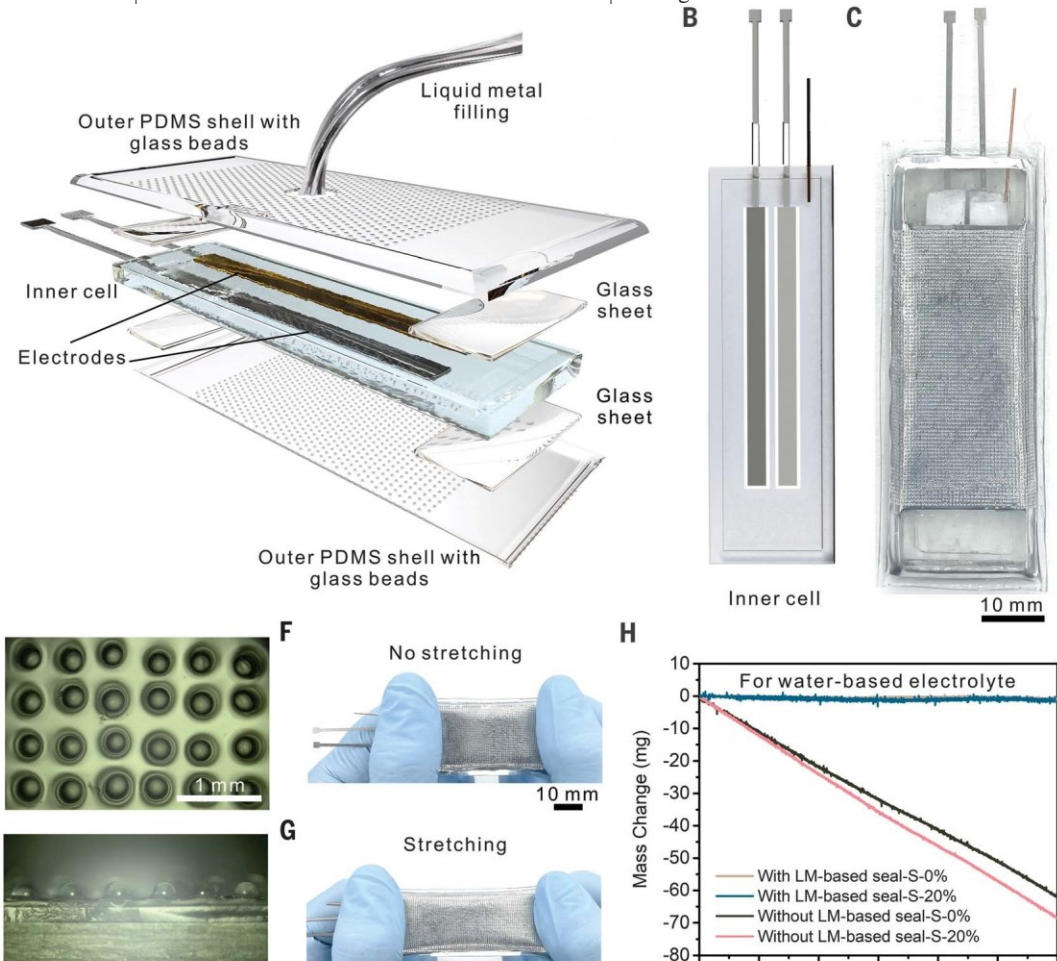
Ε

and then sealed with another PDMS sheet to form the inner cell S3B). This pristine inner cell was further bonded with four glass sheets to create places to grasp on each end of the device during stretching. It was also integrated with a copper tube that worked as an inlet for injecting the electrolyte into the inner cell. In the fabrication of the outer seal (fig. S3C), two outer PDMS sheets patterned with arrays of glass beads, which served as the spacers between the top and bottom PDMS shell of the LM encapsulation, were attached to the inner cell to form the outer PDMS chamber. With the use of the stretchable material such as PDMS as the encapsulation of the LM, the encapsulation shell might deform under the localized pressure, which will lead to the contact of the top and bottom PDMS shells and the possible failure of the hermetic seal (supplementary text, Deformation pressure and the critical role played by the spacers). The localized pressure is inevitable during the normal operation or deformation (stretching, bending, and twisting) of the soft devices, and the seal will deteriorate without the design of the spacers (30). To prevent the contact of the PDMS shells during operation, glass beads were used in the design to serve as spacers to avoid the failure of the seal from the contact of the PDMS shells. With the glass beads serving as the spacers between the PDMS shells, the PDMS between the neighboring glass beads ensure the stretchability of the integrated LMbased seal. There is a liquid-metal inlet in one of the outer PDMS sheets. EGaIn was filled into the chamber between the inner cell and outer PDMS shell through the liquidmetal inlet by means of vacuum filling. During vacuum filling, the spacers can also prevent the outer PDMS chamber from collapse, which ensures the successful filling of LM. A photograph of the prepared LIB with the LM-based seal is shown in Fig. 2C. The process for patterning the glass beads is shown in fig. S11. As shown in Fig. 2D, glass beads were patterned on the PDMS sheet and separated from each other. The crosssectional image shows that part of the glass beads was embedded into the PDMSsheet, which helpsgeneratestrongbonding (Fig. 2E). The separation between glass beads ensures the stretchability of the PDMS sheets during the stretching operation of the sealed LIB (Fig. 2, F and G). A stress-strain curve of the sealed LIB was measured and compared with that of a control LIB without the LM-based seal (fig. S12). Two stressstain curves (fig. S13) almost overlap, and the calculated Young's modulus of both the LIB with and the LIB without the LMbased seal is about 0.83 MPa, which is reasonable considering an effectively zero Young's modulus of the LM.

12

Time (h)

16



10 mm

The hermetic performance of the LM-based seal was characterized by monitoring the mass change of the LIB filled with a water-based electrolyte. The inner cell of the LIB was filled with

anelectrolytethroughtheelectrolyteinlet. After filling the inner cell, the LIB was placed onto an analytical balance, which was inside a glove box that was filled with argon, to monitor the mass change. As shown in Fig. 2H, the mass of the LIB with the LM-based seal (Fig. 2H, brown and blue curves) did not change during 24-hour measurement under both the original state and 20% strain. In comparison, the control LIB without the LM-based seal (fig. S12) exhibited rapid mass loss (Fig. 2H, black and red curves), indicating outward permeation of water vapor through PDMS sheets. The enlarged surface area of the control LIB under

with and without the LM-based seal are shown in Fig. 3A. The one with the LMbased seal exhibited a reversible capacity retention of ~90% after 140 cycles and ~72.5% after 500 cycles. The capacity decrease for the unstretched LIB is primarily due to the inevitable side reactions during the operations of LIBs rather than the gas permeation through the LM-based seal. In comparison, the control LIB without the LMbased seal (fig. S12) showed large capacity decay, with complete failure after 160 cycles owing to the outward permeation of the water vapor and inward permeation of air though the PDMS sheets (4, 31). The coulombic efficiency of the LIB with the LM-based seal was ~98%. A ofthe electrochemical comparison impedancespectroscopy (EIS) of the two LIBs at the 100th cycle is shown in Fig. 3B; the impedance of the LIB with the LM-based seal the detailed galvanostatic voltage profiles of the first nine cycles are shown in fig. S14. When the LIB was intermittently operated for only nine cycles in the same 28 days (Fig. 3D), however, the performance degradation was much smaller than that of the LIB with continuous operation. The capacity retention of the intermittently operated LIB after nine cycles in 28 days was nearly the same as that of the LIB that was continuously operated after nine cycles in ~1 day. The results indicate that the performance degradation of the LIB during the continuous cycling was mainly due to the inevitable side reactions, such as evolution of H2 and O2 from aqueous electrolytes and active materials dissolution (32, 34), rather than the permeation of gases through the seal.

The charge and discharge rate capabilities (Fig. 3E, black and blue dots) of the LIB with the

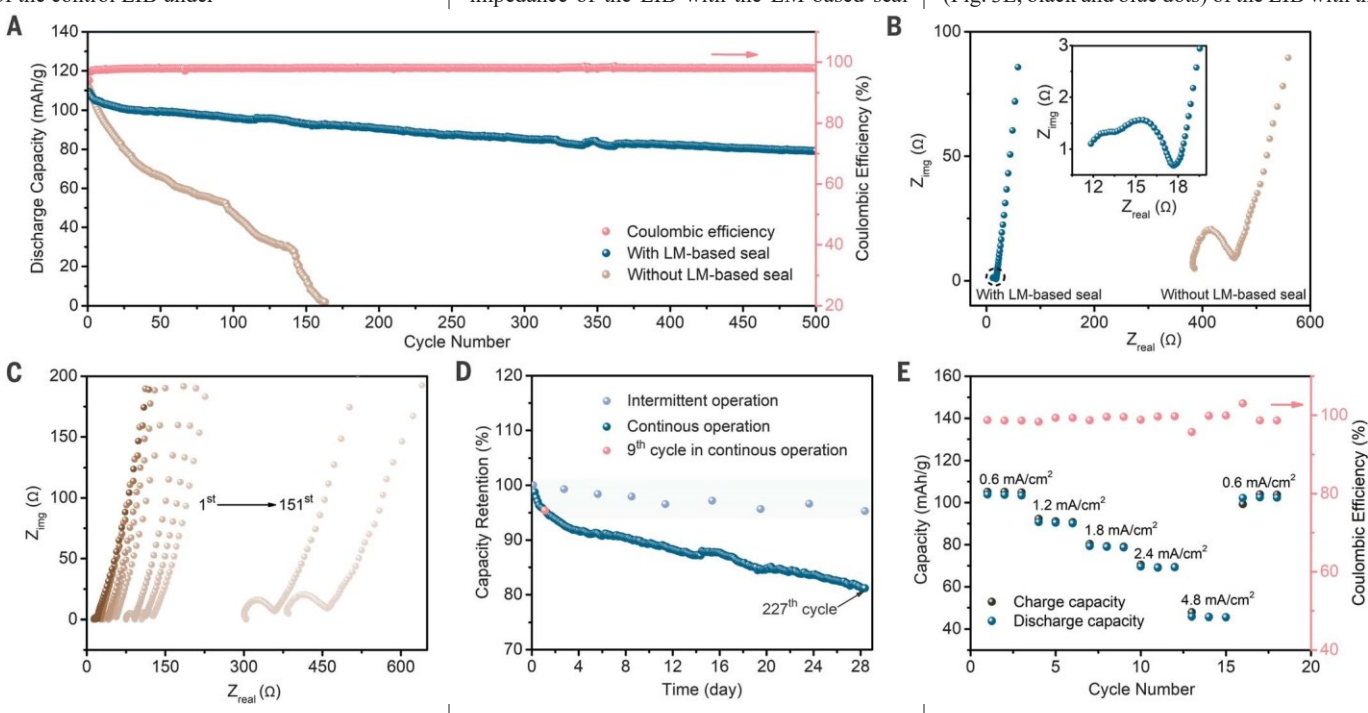


Fig. 3. Electrical performance of the stretchable LIBs under no deformation. detailed look at the low-impedance portion of the EIS for the LIB with the LM-based (A) Room-temperature-cycle life comparison at the current density of 0.6 mA/cm² seal. (C) Cycle dependent EIS for the LIB without the LM-based seal. (D) Capacity for the LIBs with and without the LM-based seal. The pink dots indicate the corresponding coulombic efficiency of the LIB with the LM-based seal. (B) Comparison of with the LM-based seal. (E) Charge and discharge rate capabilities (black and blue EIS at the 100th cycle between LIBs with and without the LM-based seal. (Inset) A dots) and coulombic efficiency (pink dots) of the LIB with the LM-based seal.

20% strain increased outward permeation of water vapor, resulting in a larger mass change than that of the LIB with no stretching.

Performance of the stretchable LIBs with the LM-based seals

The electrical performance of the stretchable LIBs with and without the LM-based seal was first characterized under no deformation. The room-temperature-cycle lives of the two LIBs

was much lower than that of the LIB without the LM-based seal. Because of the lack of the LM-based seal, the impedance of the control LIB continuously increased during the operation owing to the gradual drying out of the electrolyte and deterioration of electrodes (Fig. 3C) (4, 32, 33), resulting in the failure of the LIB. As shown in Fig. 3D, the LIB with the LM-based seal also showed a slow decline of discharge capacity during the continuous 227 cycles in 28 days, and

LM-based seal were measured at various current densities. A stable specific capacity of $\sim\!100$ mA·hour/g could be achieved at the current density of 0.6 mA/cm². Overall, it could achieve a high average specific capacity of $\sim\!90,\,80,\,70,$ and 50 mA·hour/g at 1.2, 1.8, 2.4, and 4.8 mA/cm², respectively. The decrease of thespecificcapacitywith theincreaseofcurrent density is ascribed to the electrode polarization at high currents. When the current density

Shen et al., Science 379, 488–493 (2023) 3 February 2023 4 of 6

decreased back to $0.6~\text{mA/cm}^2$, the capacity also recovered to ${\sim}100~\text{mA}\cdot\text{hour/g}$. The corresponding galvanostatic charge and discharge curves at different current densities are presented in fig. S15.

Under deformation, the electrical theLMperformanceofthestretchableLIBwith based seal was further characterized. The LIB was operated at the current density of 0.6 mA/cm² and in the potential window between 0.2 and 1.7 V. The corresponding galvanostatic chargedischarge curves of the LIB under the released state and stretched states with different strains are shown in Fig. 4A. A high reversible capacity of ~105.5 mA·hour/g was achieved for the LIB at the released state, and the capacity can be sustained at 104.8, 105.8, and 105.0 mA·hour/g under 5, 10, and 20% strain, respectively. The close overlapping of these curves indicates that this LIB can function well even under 20% strain. The EIS in Fig. 4B also shows the relatively good stability of the LIB during stretching. The tighter contact between

shown in Fig. 4B, inset (33). Furthermore, different stretching states might result in random changes of the electrochemical environment in the inner cell, such as changes of the distance between two electrodes and the position of the residual bubbles (from the possible evolution of H₂ and O₂), which causes the random differences of the diffusion impedances in the low-frequency range (Fig. 4B) (33). To further evaluate electricalperformanceoftheLIBwiththeLM-

based seal under continuously cyclic deformation, we performed cycling tests at 0.6 mA/cm² under a strain of 20%, a bending angle of 60°, and a twisting angle of 90° (Fig. 4C and fig. S16). The LIBs first operated one cycle under the released state; five cycles under stretching, bending, or twisting state; and then five cycles under the released state. The galvanostatic chargedischarge curves in Fig. 4C and the corresponding capacities remained almost the same, regardless of the deformation state of the LIB. With the use of arrays of glass beads as the spacers, the collapse of the PDMS

LMbased seal. The demonstrated stability of the LIBs with the LM-based seal offers promising potential of using such devices as the power component in stretchable electronics (fig. S17).

LM-based seals for a stretchable phase-changebased heat transfer device

Besides LIBs, this LM-based hermetic seal can also be used for other stretchable systems. In the supplementary materials, we further describe the application of this LM-based seal in a stretchable phase-change-based heat transfer device that can be used for the thermal management of stretchable electronics (fig. S18). Thermal management of stretchable electronics becomes increasingly important with the increase of the power used. Phase-change- based heat transfer devices have been widely used in modern electronics because of their superior thermal transport capability (35). The development of stretchable phase-change- based heat transfer devices, however, is limited owing to the lack of stretchable and hermetic seals. Both the inward

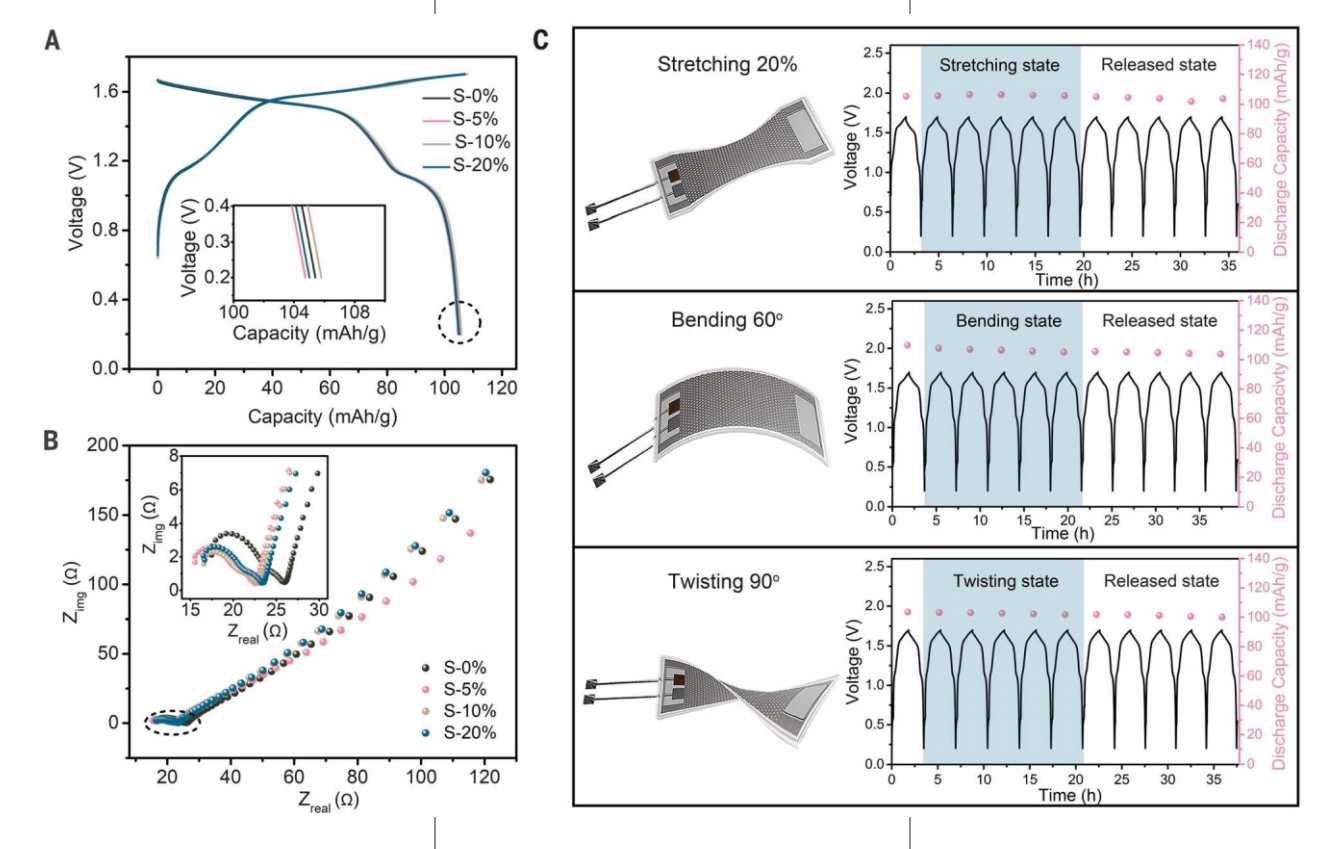


Fig. 4. Electrical performance of the stretchable LIBs with the LM-based under 0, 5, 10, and 20% strain. (Boltom inset) Detailed look at the high frequency seals under deformation. (A) Galvanostatic voltage profiles and (B) EIS of range of the EIS of the LIB. (C) The voltage profile (black curve) and discharge a LIB with the LM-based seal under 0, 5, 10, and 20% strain. The dashed shapes in capacity (pink dots) of the LIB under continuous cyclic stretching (20%), (A) and (B) indicate the enlarged area shown in the respective insets. (Top bending (60°), and twisting (90°). (Insets) The schematics of corresponding inset) Detailed look at the ends of the galvanostatic discharge curves of the LIB deformations of the LIB.

the tabs and electrodes of the LIB under stretching states might decrease the contact impedances in the high-frequency range as shells within the LM encapsulation is avoided during the deformation operation of the LIBs, which enables the stable hermetic sealing of the

permeation of noncondensable gas and the outward permeation of gasified working fluid will decrease the thermal conductivity of phasechange— based heat transfer devices. The prepared LM-based seal performed well against the permeation of ethanol (fig. S18D), which is the working fluid in the heat transfer device. The hermetic seal functions well even under heating during the stretching operation of the phase-change—based heat transfer device (fig. S18G), which showed an increased thermal conductivity of ~309 W/(m K) at 10% strain.

LM-based seals for wireless communication

Because LM is an electric conductor, it can block electromagneticcommunication into and out of the seal. In the design of a LM-based seal that allows wireless communication, we included a glass window into the original design (fig. S21, A and B). In the design, the glass window is used to transmit electromagnetic wave and at the same time provide the hermetic sealing locally. The LM surrounding the glass window provides stretchability and hermetically seals the rest of the device. To characterize the wireless communication, stretchability, permeability of thenew design of the LM-based seal, we fabricated a wireless communication device with the modified LM-based seal (fig. S21, C and D).

As shown in a schematic (fig. S22A), when a working radio frequency identification (RFID) (RD906M,906 MHz, Guangzhou Wangyuan Electronic Equipment Co.) is connected with a computer, it will send out radio signals. Without the presence of the RFID tag (CER1207, 860 to 960 MHz, Guangzhou Wangyuan Electronic Equipment Co.), no responding signals can be transmitted back to the reader, which results in only the lighting up of the red light-emitting diode (LED) on the reader and a blank screen of the computer (fig. S22, A, schematic, and B, the optical images captured during the experiment). With the presence of the wireless communication device fabricated (fig. S21D), there was communication between the RFID tag in the device and the outside reader. Both the red LED and the green LED on the reader lighted up, and there were signals displayed on the computer (fig. S22, C, schematic, and D, the optical images captured during the experiment; and movie S1). The experimental results in fig. S22E show that there was communication between the RFID tag inside the device and the outside reader even when we turned over the device (movie S2). Moreover, the wireless communication device with the modified LM-based seal could continuously communicate with the reader even under 20% strain (fig. S22F and movie S3). We also filled the inner cell of the device with deionized water containing ~2.8 wt % red dye (Wilton Industries, IL) through the copper tube and found that the filled device could still communicate with the

outside reader even under 20% strain (fig. S22G and movie S4).

The hermetic performance of the modified LM-based seal was also characterized. After filling the inner cell with a water-based electrolyte, the same one used in LIBs, the mass of the wireless communication devices with and without the modified LM-based seal was monitored through an analytical balance inside a glove box that was filled with dry argon. As shown in fig. S22H, the mass of the device with the modified LM-based seal (fig. S22H, brown and blue curves) did not change under both the original state and 20% strain state during 24-hour measurement, which is similar to the performance of the LIBs with the LMbased seal without the glass window and indicates good hermetic sealing of the modified LM-based seal. In comparison, the control device without the modified LM-based seal exhibited rapid mass loss (fig. S22H, black and red curves), which is also similar to the rapid mass loss in the LIBs without the LM-based seals.

With the integration of spacers, this work demonstrates a stretchable LM-based seal that has low permeability for blocking the transport of gases and vapors such as oxygen, water, and ethanol. In addition, LMs have metallic, thermal, chemical, and electrical properties, which may be further harnessed for additional functionality in such a barrier material that encases electronic devices. Considering the demonstrated barrier properties, this work provides a promising route for creating soft and stretchable devices with stable long-term operation.

REFERENCES AND NOTES

- 1. Y. Jiang et al., Science 375, 1411–1417 (2022).
- 2. J. T. Reeder et al., Science 377, 109–115 (2022).
- 3. S. Wang et al., Nature 555, 83-88 (2018).
- D. G. Mackanic, M. Kao, Z. Bao, Adv. Energy Mater. 10, 2001424 (2020).
- D. G. Mackanic, T.-H. Chang, Z. Huang, Y. Cui, Z. Bao, Chem. Soc. Rev. 49, 4466–4495 (2020).
- 6. P. Le Floch et al., ACS Appl. Mater. Interfaces 9, 25542–25552
- 7. P. Le Floch, S. Meixuanzi, J. Tang, J. Liu, Z. Suo, ACS Appl. Mater. Interfaces 10, 27333–27343 (2018).
- 8. M. D. Dickey, Adv. Mater. 29, 1606425 (2017).
- T. Daeneke et al., Chem. Soc. Rev. 47, 4073–4111 (2018).
- 10. A. Zavabeti et al., Science 358, 332-335 (2017).
- 11. Y. Ding et al., Adv. Mater. 32, e2002577 (2020).
- E. J. Markvicka, M. D. Bartlett, X. Huang, C. Majidi, Nat. Mater. 17, 618–624 (2018).
- S. Liu, D. S. Shah, R. Kramer-Bottiglio, Nat. Mater. 20, 851–858 (2021).
- 14. H. Wang et al., Adv. Mater. 33, e2103104 (2021).
- 15. C. Wang et al., Sci. Adv. 7, eabe3767 (2021).
- 16. Y. Lin et al., Lab Chip 17, 3043-3050 (2017).
- T. Merkel, V. Bondar, K. Nagai, B. D. Freeman, I. Pinnau, J. Polym. Sci., B, Polym. Phys. 38, 415–434 (2000).
- 18. C. Wang et al., Science 377, 517-523 (2022).
- 19. D. Jung et al., Science 373, 1022-1026 (2021).
- 20. Z. Yan et al.. Science 375, 852–859 (2022).
- H. J. Kim, B. Chen, Z. Suo, R. C. Hayward, Science 367, 773–776 (2020).
- 22. X. Xiao et al., Sci. Adv. 7, eabl3742 (2021).

- 23. Z. Zhang et al., Nature 603, 624-630 (2022).
- 24. J. R. Sempionatto et al., Nat. Biomed. Eng. 5, 737-748 (2021).
- M. Mariello, K. Kim, K. Wu, S. P. Lacour, Y. Leterrier, Adv. Mater. 34, e2201129 (2022).
- 26. M. Gu et al., Sci. Adv. 5, eaaw1879 (2019).
- 27. K. Liu et al., Joule 2, 1857-1865 (2018).
- 28. D. G. Mackanic et al., Nat. Commun. 10, 5384 (2019).
- 29. G.-M. Weng et al., Energy Storage Mater. 24, 557–564 (2020).
- N. Ochirkhuyag et al., ACS Appl. Mater. Interfaces 14, 48123– 48132 (2022).
- 31. J.-Y. Luo, W.-J. Cui, P. He, Y.-Y. Xia, Nat. Chem. 2, 760–765 (2010). 32. H. Kim et al., Chem. Rev. 114, 11788–11827 (2014).
- 32. N. Mardding at al. J. Derver Courses 400, 220742 (2020)
- 33. N. Meddings et al., J. Power Sources 480, 228742 (2020).
- 34. L. Suo et al., Science 350, 938–943 (2015).
- 35. H. Tang et al., Appl. Energy 223, 383-400 (2018).

ACKNOWLEDGMENTS

We thank Q. Kang, P. Li, X. Huang, X. Yan, and J. Gu for the help with the instruments used in preparing and characterizing LIBs. We thank W. Cheng for the help with the modeling of the spacers. Funding: This work was supported by the Innovation Program of Shanghai Municipal Education Commission (grant 2019-01-0700-02-E00069), the National Natural Science Foundation of China (51973109 and 51873105), the Zhi-Yuan Endowed fund from Shanghai Jiao Tong University, and Shanghai Jiao Tong University Overseas Study Grants. M.D.D. is grateful for the support from the National Science Foundation (ASSIST, EEC-1160483, and CMMI-2032415). W.J. acknowledges the support from MOTIE (Ministry of Trade, Industry and Energy) in Korea, under the Fostering Global Talents for Innovative Growth Program (P0008746) supervised by the Korea Institute for Advancement of Technology (KIAT). Author contributions: Q.S., J.W., W.S., M.D.D., and T.D. conceived and planned the study. Q.S., M.J., R.W., K.S., M.H.V., W.J., F.K., R.K., and F.Z. performed fabrication, testing, and characterizations. J.W., W.S., M.D.D., and T.D. supervised the study. All authors discussed and analyzed the results and contributed to the writing of the paper. Competing interests: The authors declare that they have no competing interests. Data and materials availability: All data are available in the main text or the supplementary materials. License information: Copyright © 2023 the authors, some rights reserved; exclusive licensee American Association for the Advancement of Science. No claim to original US government works.

https://www.science.org/about/sciencelicenses-journal-article-

SUPPLEMENTARY MATERIALS

science.org/doi/10.1126/science.ade7341

Materials and Methods

Supplementary Text Figs. S1 to S22

References (36, 37) Movies

S1 to S4

Submitted 8 September 2022; accepted 5 January 2023 10.1126/science.ade7341